Electronic Supplementary Material (ESI) for Green Chemistry.

Supporting Information

Preparation of nanostructured iron chromite spinel in the pure form and its catalytic activity for the selective oxidation of benzene to phenol: Experimental and DFT study

Sonu Bhandari [a, b], Rubina Khatun [a, b], Tuhin Suvra Khan [a, b], Deepak Khurana [a, b] Mukesh Kumar Poddar [a], Astha Shukla [a, b], V.V.D.N Prasad [a, b], Rajaram Bal [a, b, *]

[a] Light Stock Processing Division, CSIR-Indian Institute of Petroleum, Dehradun- 248005, Uttarakhand, India

[b] Academy of Scientific and Innovative Research (AcSIR), Ghaziabad- 201002, India

* Corresponding author E-mail- raja@iip.res.in & Tel: +91 135 2525917

S1. Catalyst characterization

The crystal structure was confirmed by powder X-ray diffraction (XRD) on a Proto Advance X-ray diffractometer fitted with a Lynx eye high-speed strip detector in the 2θ range 10-80˚ using Cu Kα (λ = 0.154 nm) as an incident beam.

The N_2 adsorption-desorption isotherms were carried out on Micromeritics ASAP 2020 Surface Area & Porosity Analyzer. The sample was degassed under vacuum at 200 ℃ for 4h before each analysis. The BET specific surface areas were determined from the adsorption data in the relative pressure (P/P_0) range of 0.06– 0.2.

TEM images were collected using a JEOL JEM 2010 DM microscope, and samples were prepared by mounting an ethanol dispersion sample on a lacey carbon formvar coated Cu grid.

Scanning Electron Microscopy (SEM) micrographs were captured on an FEI Quanta 200 F, using a tungsten filament doped with lanthanum hexaboride (LaB_6) as an X-ray source, fitted with an ETD detector with high vacuum mode, using secondary electrons and an acceleration tension of 10 or 30 kV. Samples were analyzed by spreading them on carbon tape. Energy-dispersive X-ray spectroscopy (EDX) was used in connection with SEM for the elemental analysis. SEM-elemental mapping was also collected with the spectrophotometer connected to the same instrument.

Temperature programmed reduction (TPR) and H_2 chemisorption experiments were carried out in a Micromeritics, Auto Chem II 2920 instrument connected with a thermal conductivity detector (TCD). Prior to TPR, the catalysts were also heated at 650 °C for 2 h in helium and then placed in 10% H_2/Ar with a flow rate of 40 ml min^{-1} in the temperature range of 40-1000 °C with an increment of 10 °C/min.

The surface composition and the chemical state of the samples were carried out by X-ray photoelectron spectroscopy (XPS) (KAlpha, Thermo Scientific Corp.). The monochromatized X-ray Mg Kα radiation

(1253.6 eV) was used. The core levels were calibrated by reference to the first component of the C 1s core level peak set at 284.8 eV.

Thermogravimetric analysis (TGA) of the uncalcined catalyst was carried out in a Perkin Elmer TGA 8000 hyphenated with MS by heating 4 mg samples under airflow with a temperature ramp of 10 °C min^{-1}.

Raman spectra were measured by using a HORIBA Scientific instrument equipped with OLYMPUS confocal microscope. A He/Ne power source laser with a wavelength of 633 nm was used for excitation and 2 mW laser power was used to record the spectra.

Electron paramagnetic resonance (EPR) spectra were collected at ambient temperature on a Bruker Biospin, Germany EMX micro A200-9.5/12/S/W to investigate the formation of radical species in the reaction system. The sample was placed in the capillary tube, and the experimental parameters of EPR were as follows: microwave frequency (9.38 GHz), microwave power (1.732 mW), modulation frequency (100 kHz), modulation amplitude (1.00 G) and sweep time (41 s).

Inductively coupled Plasma Atomic Emission Spectroscopic (ICP-AES) analysis was carried out by Inductively Coupled Plasma Atomic Emission Spectrometer; model: PS 3000 UV, (DRE), Leeman Labs, Inc, (USA).

DFT Method

The spin-polarized DFT calculations were performed using effective core potentials to describe the electron-core interaction along with the double numerical plus polarization (DND) basis set. The Perdew and Wang (PW91) Generalized gradient approximation (GGA) exchange-correlation functional was used.[1] For the transition state calculations, the linear synchronous transit/quadratic synchronous transit (LST/QST) method was used.[2] Convergence criteria for the DFT calculations were kept at 0.0005 eV, 0.1 eV/Å, and 0.005 Å with respect to energy, force, and atom displacement, respectively. The k-points sampling of 1x2x1 was used for all the calculations, along with thermal smearing of 0.05 Ha. $Cr_2O_3^{NP}$ and

$FeCr_2O_4$ catalysts were modelled using Cr_2O_3 (102) and $FeCr_2O_4$ (102) surface slabs, as shown in Fig. S6. Both the Cr_2O_3 (102) and $FeCr_2O_4$ (102) surface slabs were six atomic layers thick, where the bottom three layers were fixed to their bulk positions, whereas the top three layers, along with the adsorbate species, were allowed to relax during the geometry optimizations. The activation barriers (Ea) were calculated using the formula,

$E_a = E^{TS} – E_{IS}$,

where E^{TS} and E_{IS} are the energy of the transition state and initial state, respectively.

The free energy of phenyl radical desorption was calculated using the formula,

$\Delta G_{des} = (E_{des\text{-}Ph} - E_{surface\text{-}Ph}) – T(S_{des\text{-}Ph} - S_{surface\text{-}Ph})$, where $E_{des\text{-}Ph}$ is the energy of state where Ph radical is desorbed from the catalyst surface (Figure S7), $E_{surface\text{-}Ph}$ is the energy of state after the benzene C-H activation (Figure 12), whreas the $S_{des\text{-}Ph}$ and $S_{surface\text{-}Ph}$ are the entropy of above respective states. T is the reaction temperature.

Entry	Catalyst	Temp. (°C)	Oxidant	Condition	C_B (%)	S_P (%)	Ref.
1	$Pd/CeO_2/TiO_2$	80	H_2O_2	Heated under atmospheric pressure	73	95	[3]
2	$V/g\text{-}C_3N_4$	70	H_2O_2	Heated under atmospheric pressure	24.6	99.2	[4]
3	VOx/RGO	50	H_2O_2	Heated under atmospheric pressure	17.4	93.1	[5]
4	Fe-SBA-16	65	H_2O_2	Heated under atmospheric pressure	12.1	96.4	[6]
5	Fe-MFI	60	H_2O_2	Heated under atmospheric pressure	8.26	92	[7]
6	Au-Pd/CFF@TiO_2	80	H_2O_2	Heated under atmospheric pressure	46	100	[8]
7	Cu/Ti/HZSM-5	400	O_2	Tubular quartz fixed-bed micro- reactor	4.88	88	[9]
8	Fe-CN/TS-1	60	H_2O_2	Heated under photocatalytic condition	54.3	18.4	[10]
9	Fc-CO-NH-C_3N_4	60	H_2O_2	Heated under photocatalytic condition	53.3	31.7	[11]
10	**$FeCr_2O_4$**	**70**	**H_2O_2**	**Heated under atmospheric pressure**	**71.3**	**100**	**This Work**

Table S1. Literature Reports for Conversion of Benzene to Phenol

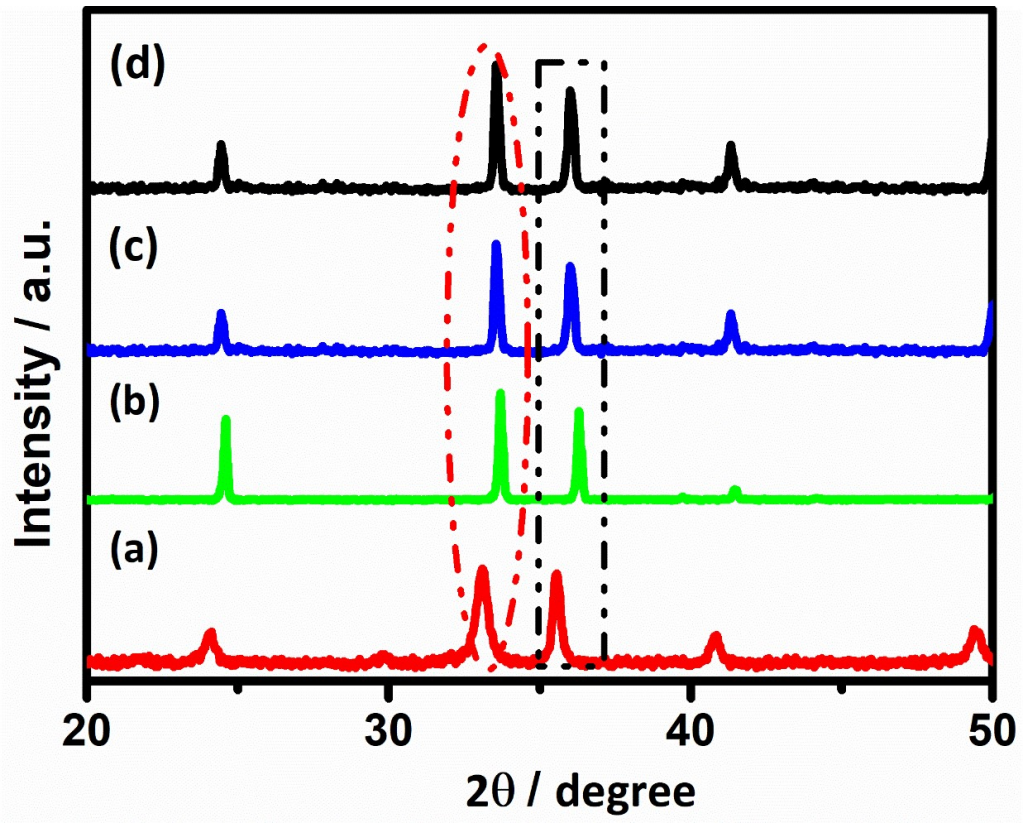

Figure S1. Powder XRD (20°-50° region) of (a) Fe_2O_3, (b) Cr_2O_3 (c) $FeCr_2O_4$ and, (d) Spent $FeCr_2O_4$ Samples

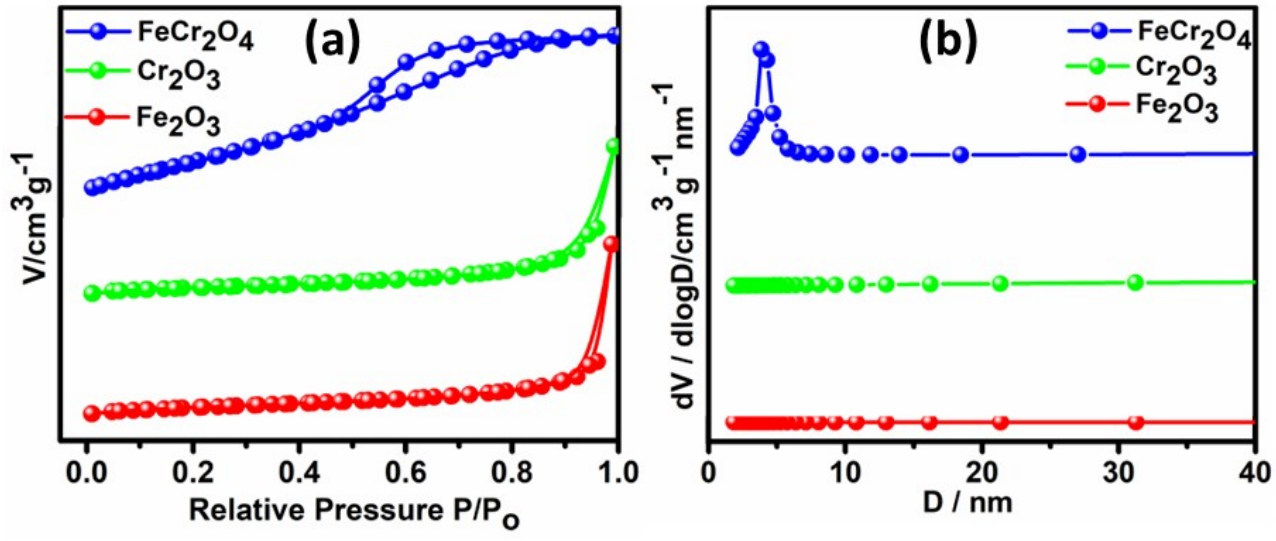

Figure S2. (a) N_2 adsorption-desorption isotherms and (b) BJH pore size distributions

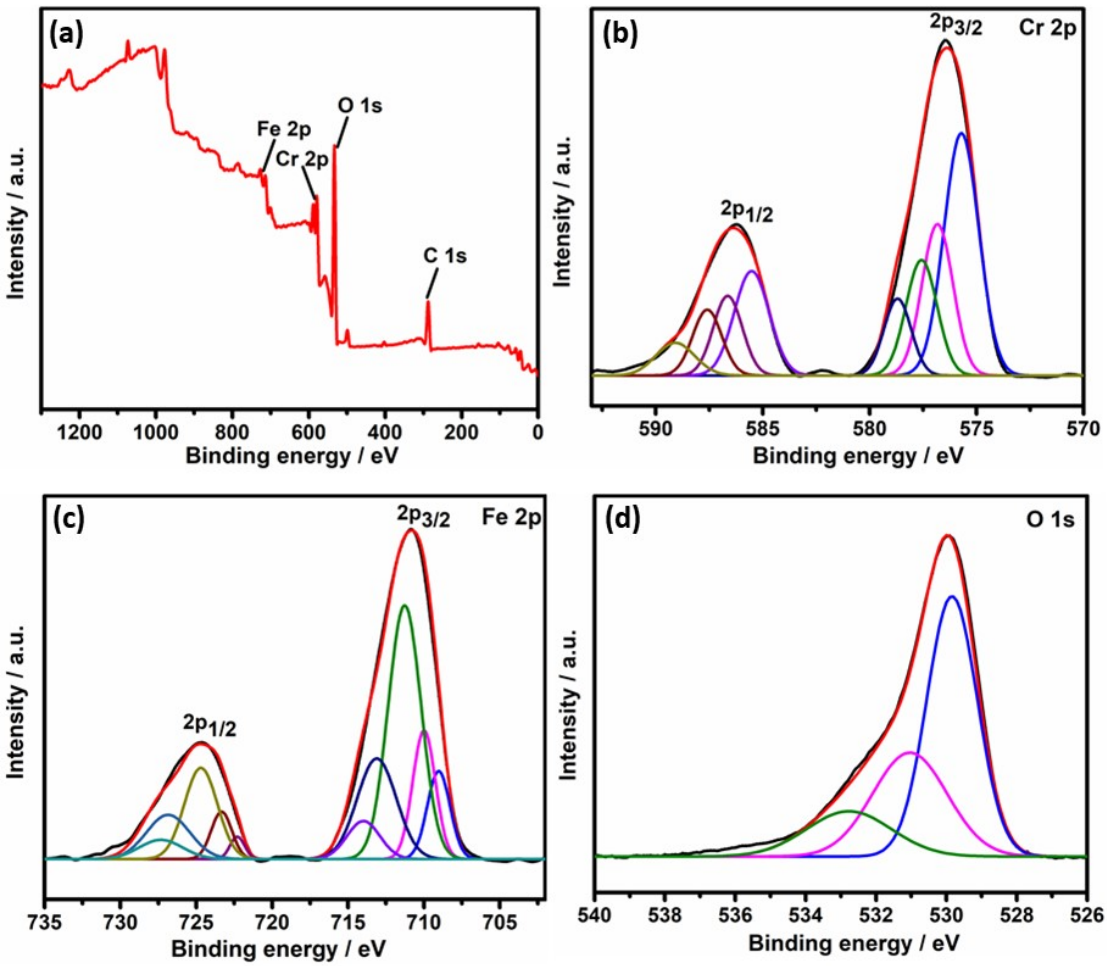

Figure S3. XPS survey (a), Cr 2p spectrum(b), Fe 2p spectrum(c) and O 1 s spectrum (d) of the spent $FeCr_2O_4$.

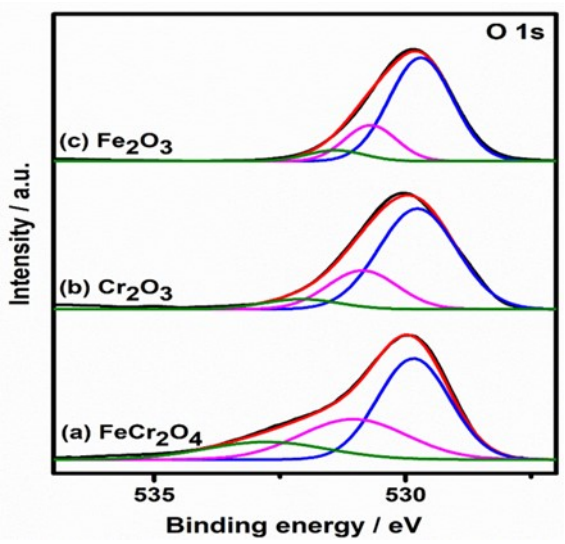

Figure S4. XPS of O 1s spectra of (a) $FeCr_2O_4$, (b) Cr_2O_3 and (c) Fe_2O_3.

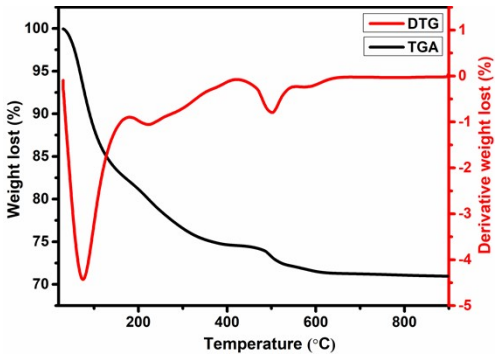

Figure S5. TGA-DTG study of the as-synthesized $FeCr_2O_4$ that has not been calcined

Table S2: Effect of different solvents

Entry	Solvent	Conversion (%)	Phenol Selectivity (%)
1	Acetonitrile	71.3	100
2	Dimethylformamide	37	57
3	Acetone	25	40
4	Ethanol	26	42

Reaction condition: 2.8 mmol benzene, 20 mg $FeCr_2O_4$, 5 ml acetonitrile, time 15 h, temperature 70 °C and 1:3 molar ratio of benzene/ H_2O_2.

Table S3. The O_{ads}/O_{latt} molar ratio and benzene reaction rate of different catalyst.

Samples	O_{ads}/O_{latt}* molar ratio	Reaction rate (mmol h^{-1} g_{cat}^{-1})
Fe_2O_3	0.28	2.09
Cr_2O_3	0.34	3.43
$FeCr_2O_4$	0.65	6.61

*O_{latt} referred to the surface lattice oxygen (O^{2-}) and the O_{ads} referred to the surface adsorbed oxygen (O_2^-, O_2^{2-} and O^-) and this surface adsorbed oxygen was related to the oxygen vacancy. This molar ratio was determined from the deconvoluted O 1s spectra of catalyst.

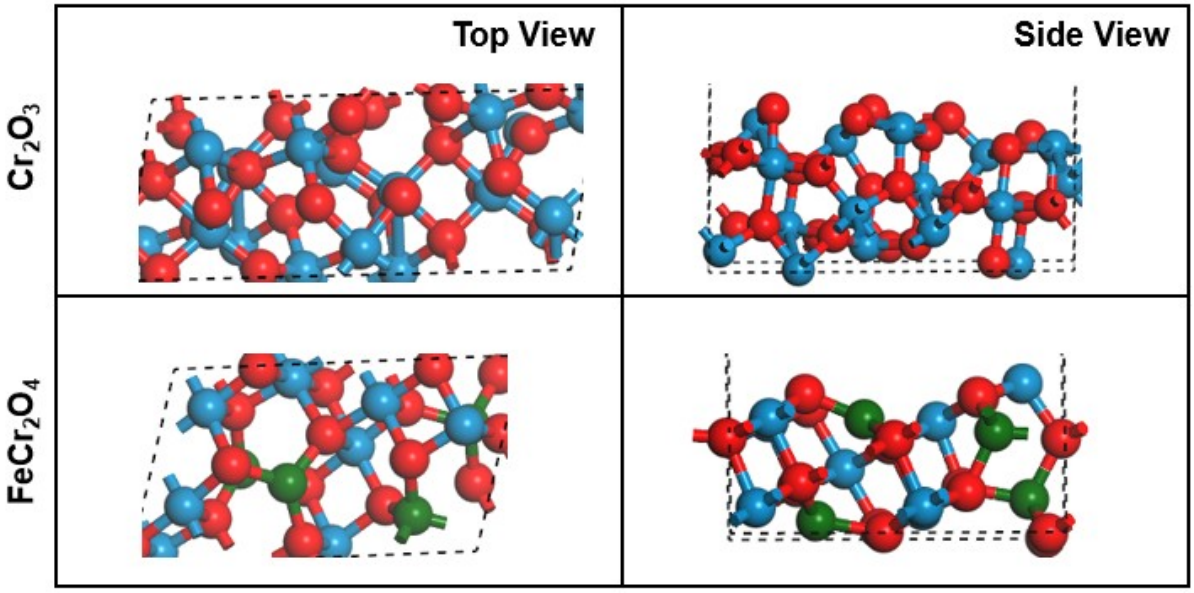

Figure S6. Top and Side view of surface Cr_2O_3 (102) and $FeCr_2O_4$ (102). Color code: Cr (blue), O (red), Fe (green) and H (white).

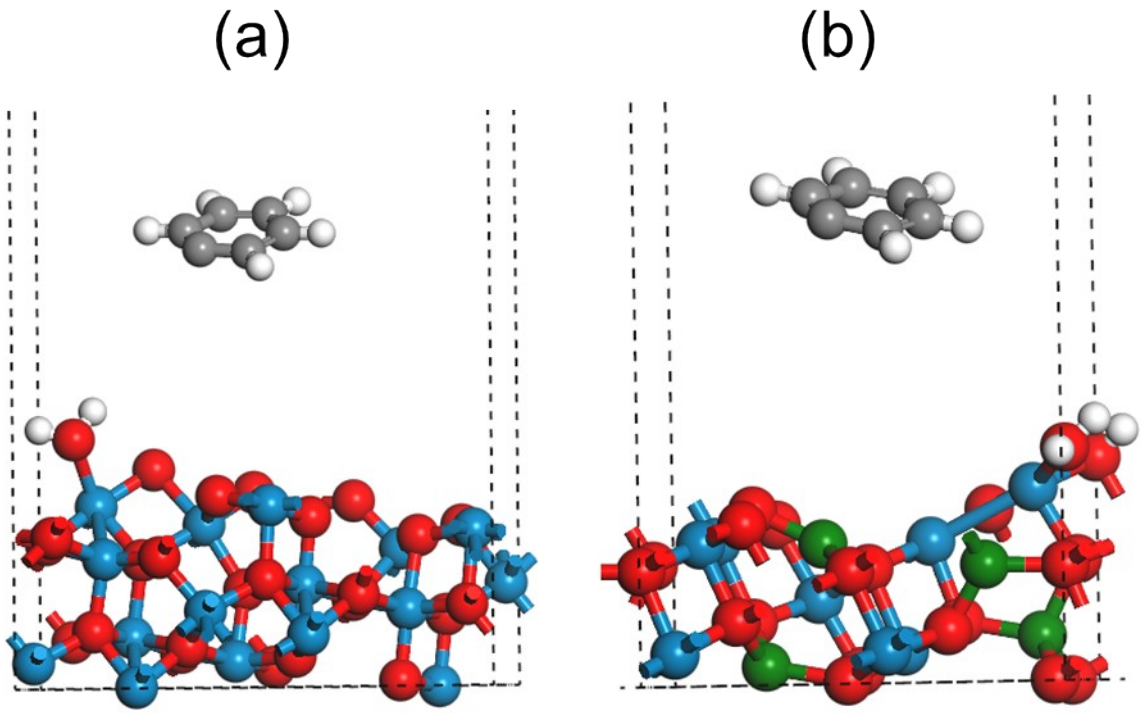

Figure S7. Surface geometry after C_6H_5 radial desorption over (a) Cr_2O_3 (102) and (b) $FeCr_2O_4$ (102). Color code: Cr (blue), O (red), Fe (green) and H (white).

Kinetics of the reaction:

The temperature dependence of the rate of the hydroxylation reaction is shown in Figure 7(B). Kinetics studies of the $FeCr_2O_4$ and Cr_2O_4 catalyst at different temperatures follow pseudo-first-order reactions. It can be applied for further assessment of the catalytic performance, and; the data revealed that the obtained experimental data fit well with calculated ones (Figure S8). Therefore, the equation of kinetic for this reaction can be manifested as

$-\ln \frac{A}{A_0} = kt$, where A_0 and A are the initial and final benzene concentration at time t; apparent rate constant is represented by k; t is the reaction time, respectively.

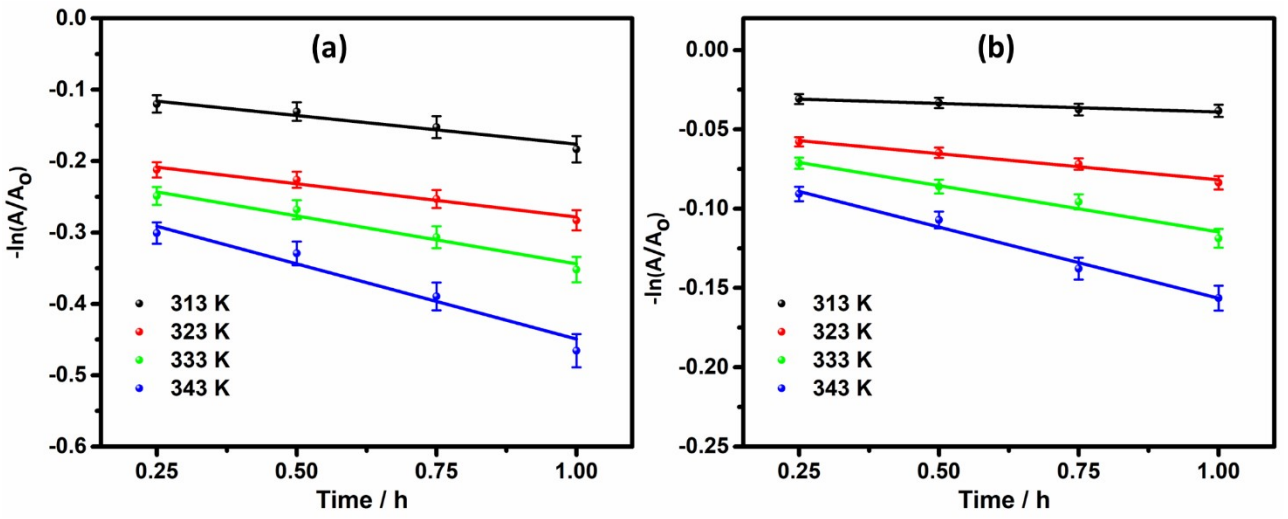

Figure S8. $\ln(A/A_0)$ versus reaction time of the oxidation of benzene carried out at different temperatures over (a) $FeCr_2O_4$ and (b) Cr_2O_3 nanoparticles.

From the slopes of the line of best fit, the apparent rate constant values for the reactions were calculated at 40, 50, 60, and 70 °C.

Additionally, the apparent activation energy was calculated using the Arrhenius equation. and expressed as;

$$\ln k = \ln A - \frac{E_a}{RT}$$

Where the reaction temperature is T, the pre-exponential factor is A, and the molar gas constant is R. The slope of the line of best fit obtained by plotting lnk vs 1000/T (Figure S9) yielded the value of the activation energy (E_a) of 114 and 127.4 kJ/mol for $FeCr_2O_4$ and Cr_2O_3, respectively.

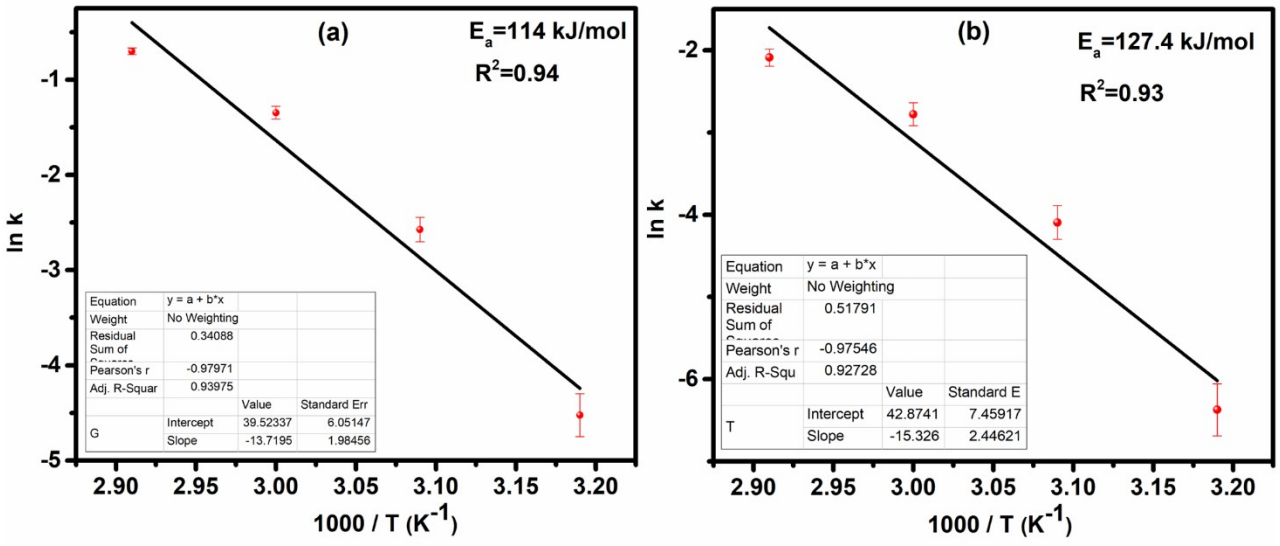

Figure S9. Arrhenius plot showing benzene oxidation reactions over (a) $FeCr_2O_4$ and (b) Cr_2O_3 nanoparticles at various temperatures.

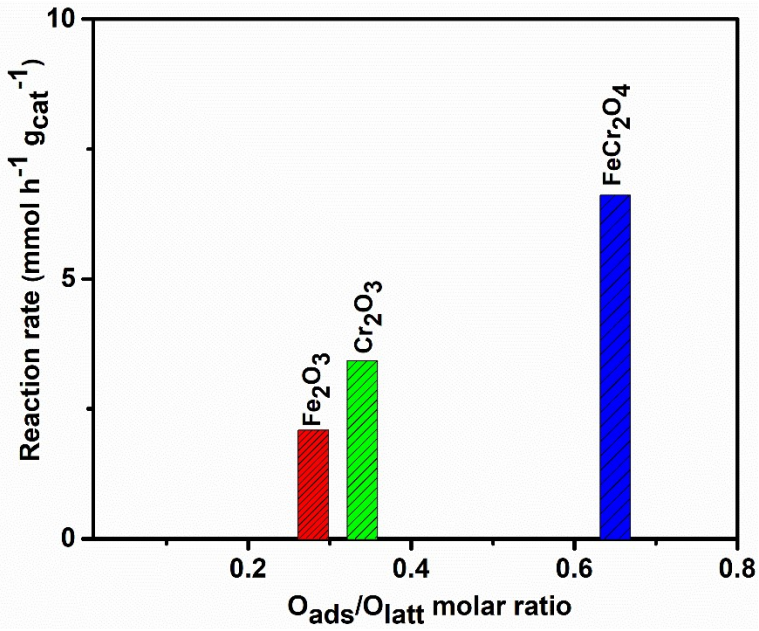

Figure S10. Correlation of O_{ads}/O_{latt} molar ratio versus Reaction rate over $FeCr_2O_4$, Cr_2O_3 and Fe_2O_3 nanostructured catalyst.

References

1 John P. Perdew and Yue Wang, *Physical Review B - Condensed Matter and Materials Physics B*, 1992, **45**, 244–248.

2 T. A. Halgren and W. N. Lipscomb, *Chem. Phys. Lett.*, 1977, **49**, 225–232.

3 X. Ma, R. Dang, Z. Liu, F. Yang, H. Li, T. Guo and J. Luo, *Chem. Eng. Sci.*, 2020, **211**, 115274.

4 C. Wang, L. Hu, M. Wang, Y. Ren, B. Yue and H. He, *Cuihua Xuebao/Chin. J. Catal.*, 2016, **37**, 2003–2008.

5 Y. Dong, X. Niu, W. Song, D. Wang, L. Chen, F. Yuan and Y. Zhu, *Catalysts*, 2016, **6**, 1–16.

6 M. Jourshabani, A. Badiei, Z. Shariatinia, N. Lashgari and G. Mohammadi Ziarani, *Ind. Eng. Chem. Res.*, 2016, **55**, 3900–3908.

7 P. Xiao, Y. Wang, J. N. Kondo and T. Yokoi, *Appl. Catal. A, Gen.*, 2019, **579**, 159–167.

8 S. M. Hosseini, M. Ghiaci, S. A. Kulinich, W. Wunderlich, B. H. Monjezi, Y. Ghorbani, H. S. Ghaziaskar and A. Javaheri Koupaei, *Appl. Surf. Sci.*, 2020, **506**, 144644.

9 A. Okemoto, Y. H. Tsukano, A. Utsunomiya, K. Taniya, Y. Ichihashi and S. Nishiyama, *J. Mol. Catal., A: Chem.*, 2016, **411**, 372–376.

10 X. Ye, Y. Cui, X. Qiu and X. Wang, *Appl. Catal. B*, 2014, **152–153**, 383–389.

11 X. Ye, Y. Zheng and X. Wang, *Chin. J. Chem.*, 2014, **32**, 498–506.